Compression Behavior of ±45°-Dominated Laminates with a Circular Hole or Impact Damage

Mark J. Shuart* and Jerry G. Williams*
NASA Langley Research Center, Hampton, Virginia

An investigation of the compression failure characteristics of ±45°-dominated laminates with a circular hole or impact damage was conducted. Graphite-epoxy laminates consisting of all ±45° plies and of ±45° and 90° plies were evaluated. In-plane shearing between the fibers and matrix (i.e, matrix shearing) was found to be the primary compression failure mechanism for an all ±45° laminate with a hole. The failure mechanism for the ±45°-dominated laminates with a hole appeared to be a combination of delamination and matrix shearing. The compression failure stresses and strains for both the all ±45° laminate and the ±45°-dominated laminates were unaffected by impact damage at an energy level of 5.5 J when compared to results for undamaged control specimens. The failure stresses and strains for all laminates with impact damage at energy levels of 17.0 or 34.3 J were significantly lower than the corresponding data for the undamaged control specimens. The failure stresses and strains for these impact-damaged specimens were independent of the percentage of 90° plies in the laminate.

Introduction

COMPOSITE materials are being widely used in aircraft structures. Graphite-epoxy has been successfully used in light- and medium-loaded secondary structures on commercial aircraft. Current investigations are considering the use of graphite-epoxy for heavily loaded primary structural components such as wings and fuselages. Tests have shown that the compression strength of heavily loaded wing and fuselage skins can be reduced by local discontinuities such as holes or impact damage.[1] Design concepts for compression-loaded composite components are being studied to reduce the effects of discontinuities; such concepts are described as damage tolerant. Leading damage-tolerant concepts for heavily loaded graphite-epoxy structures incorporate a low-axial/high-shear stiffness skin element composed primarily of ±45° plies. This type of skin element has been shown to be more tolerant to impact damage than elements having high axial stiffness.[2]

The current investigation was conducted to study the failure characteristics of compression-loaded ±45°-dominated graphite-epoxy laminates with a circular hole or impact damage; the results from this investigation are reported herein. The compressive behavior of ±45°-dominated graphite-epoxy laminates with various percentages of 90° plies through the thickness is described and is compared to the all ±45° laminate response. The percentage of 90° plies in the ±45°-dominated laminates is 8-33% of the laminate thickness. The failure mechanisms for the laminates in this study are discussed. The effect of hole diameter or impact speed on the compression strength of all ±45° and of ±45°-dominated graphite-epoxy laminates is reported. A closed-form anisotropic plate analysis[3] is used to determine the stress distribution around a hole. Birefringent composite specimens with a circular hole were also tested in compression to obtain qualitative data about laminate stress distribution and failure mode.

Test Specimens

The graphite-epoxy composite specimens tested in this investigation were fabricated from commercially available unidirectional Hercules AS4† graphite fiber tapes preimpregnated with 450 K cure Hercules 3502† thermosetting epoxy resin. Typical lamina elastic properties for this graphite-epoxy system are given in Table 1. The tapes were laid to form 48 ply laminates approximately 0.64 cm thick and the laminate stacking sequences are listed in Table 2.

The laminates were cured in an autoclave using the manufacturer's recommended procedure. Following cure, the laminates were ultrasonically C-scanned to establish specimen quality and then cut into test specimens. All graphite-epoxy specimens were 25.4 cm long and 12.7 cm wide. The loaded ends of each specimen were machined flat and parallel to permit uniform compressive loading. Centrally located circular holes were machined into some of the specimens with diamond impregnated core drills.

Transparent birefringent composite specimens were also tested in this investigation. The specimens were fabricated using the procedure described in Ref. 4 from commercially available J.P. Stevens and Co. style 3733 glass cloth with an S-190† finish. The cloth was preimpregnated with Marblette Corp. Maraset 658/558† epoxy resin. The stacking sequence for the birefringent specimens was $[+45_4/-45_4]_{2S}$. A centrally located circular hole was machined into each specimen using diamond impregnated core drills. The birefringent composite specimens were 15.2 cm long, 7.6 cm wide, and 0.20 cm thick.

Apparatus and Tests

Test specimens were loaded in axial compression using a 1.33 MN capacity hydraulic testing machine. The loaded ends of the specimen were clamped by fixtures during testing and the sides were simply supported by restraints to prevent the specimen from buckling as a wide column. A typical specimen mounted in the support fixture is shown in Fig. 1.

Electrical resistance strain gages were used to monitor strains and dc differential transformers were used to monitor longitudinal displacements of the ends. Electrical signals from the instrumentation and the corresponding applied loads were recorded on magnetic tape at regular time intervals during the test. The locations of the back-to-back gages used to monitor the far-field (i.e., removed from the discontinuity) laminate strain are shown in Fig. 1.

Received April 30, 1984; presented as Paper 84-0848 at the AIAA/ASME/AHS 25th Structures, Structural Dynamics and Materials Conference, Palm Springs, CA, May 14-16, 1984; revision received March 1985. This paper is declared a work of the U.S. Government and therefore is in the public domain.

*Aerospace Engineer, Structural Mechanics Branch, Structures and Dynamics Division. Member AIAA.

†Identification of commercial products and companies in this report is used to describe adequately the test materials. The identification of these commercial products does not constitute endorsement, expressed or implied, of such products by the National Aeronautics and Space Administration.

Table 1 Graphite-epoxy lamina properties

Longitudinal Young's modulus, E_1	127.6 GPa
Transverse Young's modulus, E_2	11.3 GPa
Shear modulus, G_{12}	6.0 GPa
Major Poisson's ratio, ν_{12}	0.30
Nominal lamina thickness, t	0.13 mm

Table 2 Laminate stacking sequences

Laminate (90° plies, %)	Stacking sequence
A (0)	$[(\pm 45/\mp 45)_6]_s$
B (0)	$[(\pm 45)_{12}]_s$
C (8)	$[(\pm 45/\mp 45)_4/90/\pm 45/\mp 45/90/\pm 45]_s$
D (17)	$[(\pm 45/\mp 45)_3/90/\pm 45/\mp 45/90_2/\pm 45/\mp 45/90]_s$
E (25)	$[\pm 45/\mp 45/(\pm 45/\mp 45/90_2)_3 \pm 45]_s$
F (33)	$[\pm 45/\mp 45/(\pm 45/\mp 45/90_3)_2/\pm 45/\mp 45/90_2]_s$

A procedure for impacting graphite-epoxy components detailed in Ref. 1 was also used in the current investigation. Aluminum spheres 1.27 cm in diameter were used as impact projectiles. These spheres were propelled by a compressed-air gun equipped with an electronic detector to measure projectile speed. A schematic drawing of the air gun and a description of its operation are also given in Ref. 1.

All specimens were tested to failure by slowly applying a compressive load to simulate a static loading condition. Three types of graphite-epoxy specimens were tested: control specimens (specimens without holes or impact damage), specimens with a single circular hole, and specimens that had been subjected to impact damage prior to loading. Five control specimens were loaded to failure to determine their compressive stress-strain behavior and failure characteristics. One specimen for each of the laminates A-F were tested; a control specimen test for laminate B was not conducted. Sixteen specimens, each with a single circular hole,were loaded to failure to determine the effect of holes on the compressive response. Hole diameters were 0.64-5.08 cm (ratios of hole diameter to plate width of 0.05-0.40). Fifteen specimens were impacted without any applied compressive load and then loaded to failure to determine the effect of impact damage on the compressive response. The 1.27 cm diameter aluminum projectiles were directed normal to the plane of the specimen at speeds of approximately 61, 107, or 152 m/s, which correspond to impact energies of 5.5, 17.0, and 34.3 J, respectively. All specimens were impacted at the center of the test section as indicated in Fig. 1. Impact-damaged specimens were ultrasonically C-scanned prior to loading.

Two birefringent composite specimens with a single circular hole were also tested in compression. The hole diameters were 1.27 and 1.91 cm (diameter-to-width ratio of 0.17 and 0.25, respectively).

Results and Discussion

Control Specimens

The compressive stress-strain response is shown in Fig. 2 for laminates A and C-F. Three trends were observed by comparing the response of ±45°-dominated laminates with the laminate A response. First, the response of the ±45°-dominated laminates is closer to linear than the response of the all ±45° laminate. Second, the failure strain for the ±45°-dominated laminates is lower than the failure strain for laminate A. Third, the failure stress for the ±45°-dominated laminates is 44-61% higher than the strength for the all ±45° laminate A. The response of the ±45°-dominated laminates is affected by the in-plane lateral restraint on laminate deformation that occurs when 90° plies

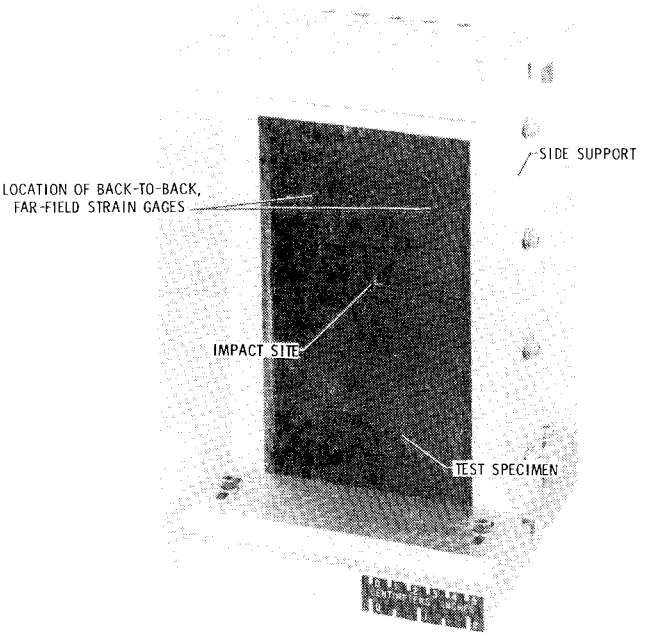

Fig. 1 Graphite-epoxy specimen in test fixture.

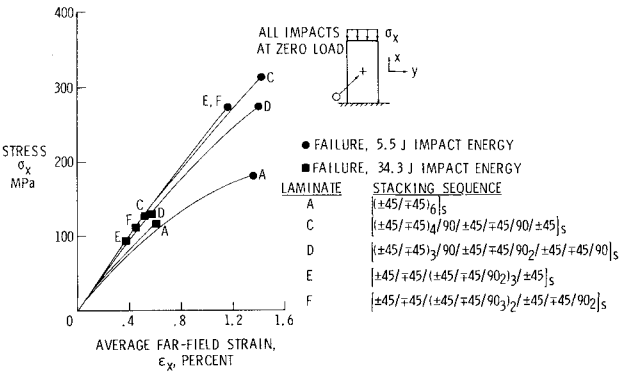

Fig. 2 Compressive stress-strain behavior for control specimens.

are added to an all ±45° laminate. For a $[\pm 45/90]_s$ class laminate under longitudinal load, the 90° plies restrain in-plane shearing in the ±45° plies. The effects on the linear elastic material properties of adding 90° plies to an all ±45° laminate are shown in Fig. 3. Results were obtained using laminate theory and the test laminates designated A-F are indicated on a separate scale. As illustrated in the figure, the longitudinal Young's modulus E_x for a $[\pm 45/90]_s$ class laminate is greater than the corresponding property for an all ±45° laminate because of the in-plane lateral restraint. Also, the shear modulus G_{xy} for a $[\pm 45/90]_s$ class laminate is less than the corresponding property for an all ±45° laminate. The in-plane lateral restraint significantly affects the transverse Young's modulus E_y and Poisson's ratio ν_{xy} as shown in Fig. 3. The transverse Young's modulus for laminate F is almost three times the same property for laminate A and the Poisson's ratio for laminate F is approximately half the corresponding laminate A property.

The failure stress and strain data for control laminates A and C-F are presented in Table 3. The failure strain is the average measurement from two pair of back-to-back far-field strain gages recorded at failure. The far-field failure strain for laminate A was calculated using laminate end shortening because this value exceeded the capability of the strain gages. Failure strains for other control laminates were calculated using this technique and the calculated values were 6-10% higher than the values obtained from far-field strain

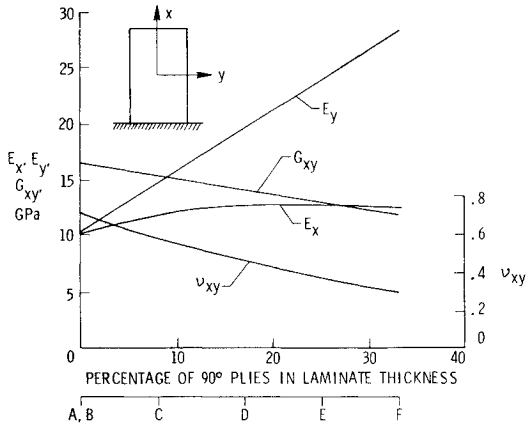

Fig. 3 Elastic properties for ±45°-dominated laminates.

Table 3 Compression failure data for control specimens and specimens with circular holes

Laminate,[a] (90° plies, %)	Laminate thickness, cm	Hole diameter, cm	Failure stress, MPa	Failure strain, %
A (0)	0.65	0.	192	1.97[b]
	0.66	2.54	144	0.81
	0.65	5.08	107	0.52
B (0)	0.64	0.64	181	1.45
	0.64	1.27	176	1.08
	0.63	2.54	159	0.92
	0.64	3.81	137	0.73
	0.65	5.08	113	0.58
C (8)	0.67	0.	293	1.34
	0.68	2.54	195	0.83
	0.67	5.08	143	0.61
D (17)	0.68	0.	276	1.43
	0.69	2.54	192	0.88
	0.68	5.08	137	0.61
E (25)	0.63	0.	280	1.15
	0.65	2.54	187	0.76
	0.65	5.08	131	0.55
F (33)	0.67	0.	309	1.34
	0.67	2.54	195	0.78
	0.67	5.08	134	0.55

[a]See Table 2 for stacking sequence. [b]Failure strain calculated using lamiante end shortening and original length rather than from strain gage.

gages. For the all ±45° laminate, failure corresponds to the near-zero slope of the stress-strain curve (see laminate A response in Fig. 2). For the ±45°-dominated laminates, failure corresponds to a catastrophic event that terminates the load carrying capability of the laminate. By inspecting the failed specimens the failure mechanism for laminate A was observed to be matrix shearing. The failure mechanism for the ±45°-dominated laminates was observed to be a combination of matrix shearing and delamination. The matrix-shearing mechanism will be defined and discussed in the next section.

Circular Hole Specimens

Analytical Results

The analytical procedure described in Ref. 3 was used in this investigation to calculate the laminate stress and strain fields in the vicinity of a circular hole assuming the laminate to be an infinite anisotropic plate. Ply stresses in the principal material coordinate system were determined using laminate theory. These infinite plate results approximate the finite plate results when the finite width effects are negligible. For this study, a reasonable assumption was to neglect

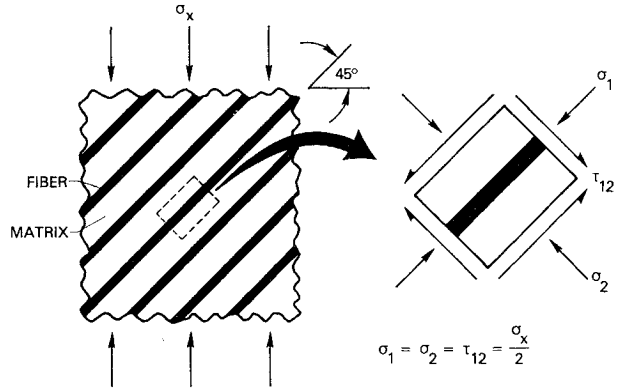

Fig. 4 Stress transformation for +45° lamina.

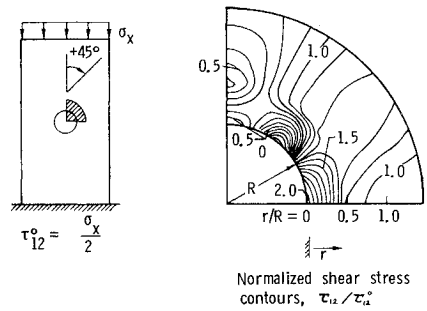

Fig. 5 Shear stress distribution in principal directions for a compression-loaded +45° ply in an all ±45° laminate.

such finite width effects, since the in-plane stress concentration was localized in the vicinity of the hole. This assumption is supported by the results in Ref. 5 for a $[\pm 45]_s$ laminate with a hole.

The stresses in the principal or 1, 2 material directions for a 45° ply in a compression loaded all ±45° laminate without a hole are shown in Fig. 4. For this loading, the in-plane shear stress τ_{12} is a maximum on elements oriented 45° to the applied load. The fiber/matrix interface for this layer is also oriented at 45° to the applied load. Hence, the maximum shear stress acts in a plane coincident with the fiber/matrix interface causing significant shear stresses at that interface and in the epoxy matrix between fibers. This shearing mechanism is subsequently referred to as matrix shearing.

The shear stress distribution in the principal material directions for a ±45° ply in an all ±45° laminate with a circular hole is shown in Fig. 5. The contours of constant shear stress are normalized by the far-field shear stress τ^0_{12} for this layer. The shear stress is a maximum at the point where the hole boundary intersects the horizontal centerline of the specimen and the shear stress concentration factor is calculated to be 2.0. As discussed in the previous paragraph, this shear stress acts in the epoxy matrix between fibers. The shear strength of an epoxy resin (Narmco 5208) similar to the resin used in this study is recorded[6] to be 60 MPa and the shear stresses at the edge of the hole are predicted to be greater than or equal to this strength. The high shear stress at the edge of the hole could initiate a local matrix shearing failure. The density of stress contours at the hole boundary indicates that the shear stress at this boundary decreases rapidly from the maximum value until it is negligible at 45° to the load axis.

The effect of adding 90° plies to an all ±45° laminate on the lamina shear stress distribution near a hole is shown in Fig. 6. Laminate loading and the location of the shear stress concentration are shown in Fig. 6a. The contours of constant shear stress in the principal material direction for a 45° ply

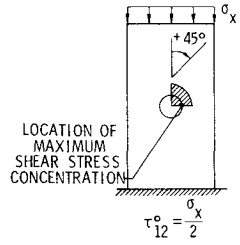

a) Loading.

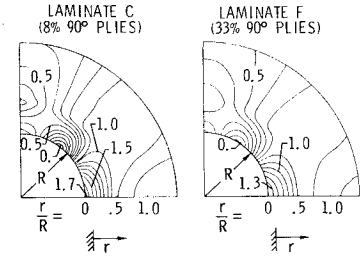

b) Normalized shear stress contours, τ_{12}/τ^0_{12}.

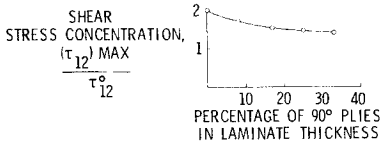

c) Shear stress concentration in a +45° ply for a ±45°-dominated laminate with a hole.

Fig. 6 Shear stress distribution in principal directions for a compression-loaded +45° ply in a ±45°-dominated laminate.

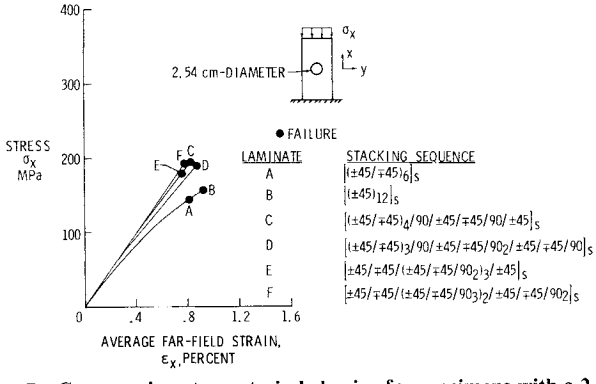

Fig. 7 Compression stress-strain behavior for specimens with a 2.54 cm diameter hole.

in laminates C and F are shown in Fig. 6b. These contours can be compared to results for the all ±45° laminate (laminate A or B) shown in Fig. 5. The results shown in Fig. 6b also indicate that the shear stress at the hole boundary for each ±45°-dominated laminate decreases from the maximum value until it is negligible at 45° to the load axis. The shear stress concentration in a +45° ply for laminate C or F is lower than the shear stress concentration in a +45° ply for the all ±45° laminate. The shear stress concentration in a +45° ply for all the laminates studied in this investigation is shown in Fig. 6c. The plot shows a gradual reduction in the shear stress concentration as the percentage of 90° plies in the laminate is increased.

Experimental Results

Compressive stress-strain behavior for each test laminate with a 2.54 cm diameter hole (ratio of hole diameter to plate width of 0.20) are shown in Fig. 7. Failure stresses and

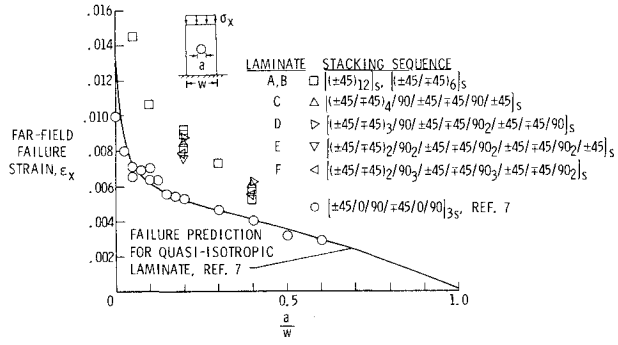

Fig. 8 Failure strain as a function of hole diameter for all ±45° and ±45°-dominated laminates.

a) Control specimen.

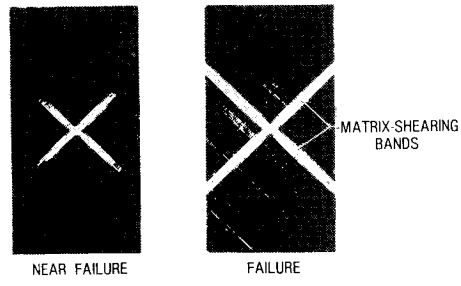

b) Specimen with 0.64 cm diameter hole.

Fig. 9 C-scan results for a $[(\pm45)_{12}]_s$ laminate.

strains for all specimens with circular holes are presented in Table 3. Similar to the results for the control specimens, the ±45°-dominated laminate response (laminates C-F) is stiffer and more linear than the all ±45° laminate response (laminates A and B). Also, the failure stresses for laminates C-F are higher than the corresponding stresses for laminates A and B. However, the far-field failure strains for laminates C-F are approximately the same as those for laminates A and B. A similar trend is also observed in Table 3 for the failure strain of laminates with a 5.08 cm diameter hole. These data suggest that the ultimate strain may be approximately equal for ±45°-dominated and all ±45° laminates with a similar hole. However, the ±45°-dominated laminates can carry greater load (because of their higher stiffness) than the all ±45° laminates at the same strain level.

Far-field strain at failure as a function of the ratio of hole diameter to plate width a/w are presented in Fig. 8. For comparison with a fiber-dominated laminate, the predicted failure based on analysis (solid curve) and the data (circular symbols) are shown on the figure for a quasi-isotropic laminate taken from Ref. 7. Similar to the failure strain for the quasi-isotropic laminate, the failure strain for laminates A and B (square symbols) and laminates C-F (triangular symbols) decreases as the hole diameter increases. However, the failure strains for laminates A-F are substantially higher than the failure strains for the quasi-isotropic laminate with the same hole diameter. For example, at $a/w = 0.05$ the

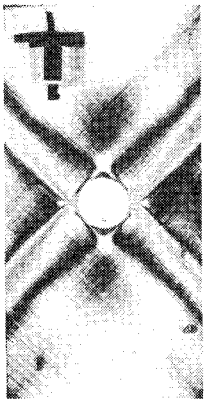

a) Specimen with 1.91 cm diameter hole near failure.

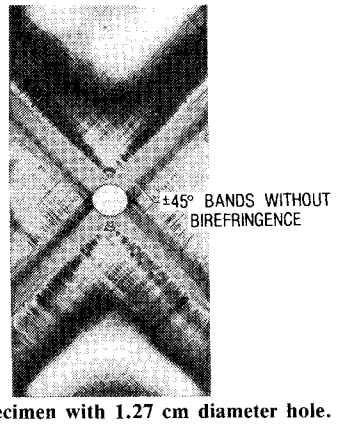

b) Failed specimen with 1.27 cm diameter hole.

Fig. 10 $[+45_4/-45_4]_{2s}$ birefringent specimen illuminated with polarized light.

failure strain for laminate B is twice the failure strain for the quasi-isotropic laminate. As mentioned above, the failure strain is approximately the same for the ±45°-dominated and the all ±45° laminates with holes at $a/w=0.2$ and 0.4.

Photographs of C-scan results for an all ±45° control specimen and for an all ±45° specimen with a 0.64 cm diameter hole following loading are shown in Fig. 9. Local failure is indicated by the white regions on the photographs. For the control specimen (Fig. 9a), a diamond-shaped region located in the center of the specimen has failed and, in addition, ±45° bands of failure extend to the edge of the specimen. For the specimen with a circular hole (Fig. 9b), the C-scan results show that failure initiates at the hole boundary and grows in bands oriented at ±45° toward the simply supported edges as the specimen is loaded near failure. The same specimen was then loaded to failure and the C-scan results show that bands of failure approximately the width of the hole diameter extend to the simply supported edges. These bands of failure were typical for every all ±45° specimen with a hole. When a failed all ±45° specimen is destructively examined using a deplying technique,[8] in-plane matrix shearing was exhibited with little evidence of fiber breakage. The ±45° bands of failure shown by the C-scans for the control specimen and for the specimen with a hole illustrate that matrix shearing appears to be the primary compressive failure mechanism for both of these all ±45° specimens.

The failure characteristics of tension-loaded all ±45° laminates have been studied using different materials.[9-12] In all cases, the laminate failure initially propagated along lines oriented ±45° to the load axis and was caused by matrix shearing. The common failure mode reported in these references indicates that the matrix-shearing failure mechanism is independent of the material system for tension-

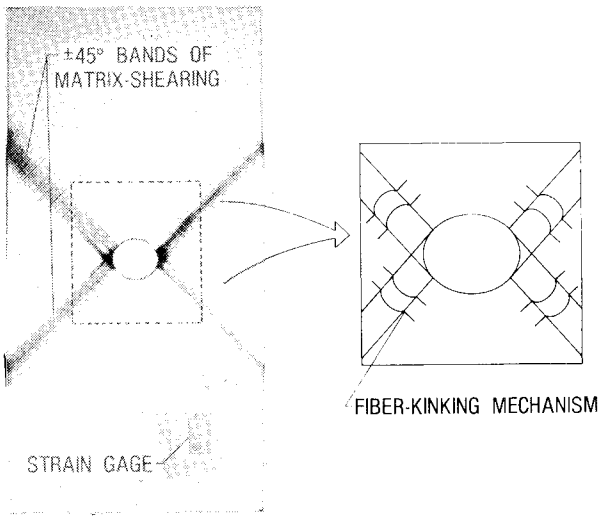

Fig. 11 Failed $[+45_4/-45_4]_{2s}$ birefringent specimen illuminated with white light (hole diameter is 1.27 cm).

loaded all ±45° laminates. This mechanism is also characteristic of the graphite-epoxy material system and glass-epoxy birefringent material system used in this study of compression-loaded laminates.

Glass-epoxy all ±45° birefringent specimens with a circular hole are shown in Figs. 10 and 11. Following loading, the specimens in Fig. 10 were illuminated with polarized light to observe the regions of stress concentration. A specimen loaded near failure is shown in Fig. 10a, and one loaded to failure in Fig. 10b. The photograph of the specimen with a 1.91 cm diameter hole (Fig. 10a) shows ±45° fringe bands between the hole and simply supported edges that represent regions of high residual stress. The isochromatic fringes indicate that the maximum stresses in these bands occur at the two locations where the hole boundary intersects the horizontal centerline of the specimen, which are the locations where failure initiated. The photographs of the specimen with a 1.27 cm diameter hole (Fig. 10b) also shows similar bands, but these bands are not birefringent. The lack of birefringence is caused by internal failure, such as delamination and in-plane shearing, that has disrupted the light path and destroyed the birefringency property. The specimen with a 1.27 cm diameter hole is shown in Fig. 11 illuminated with white light. The damaged regions are shown as ±45° dark lines. Visual examination of the specimen indicates that failure is most severe at the two locations where the hole boundary intersects the horizontal centerline of the specimen. Although significant failure is observed elsewhere within the ±45° bands and at the simply supported edges, this failure was observed to occur subsequent to that at the hole boundary. Closer inspection of the failed regions reveals that a fiber-kinking mechanism has occurred at the boundaries of the matrix-shearing bands. A sketch illustrating this fiber-kinking mechanism in the hole boundary region is shown in Fig. 11. The kinking results from a +45° layer restraining the in-plane shearing that occurs in an adjacent −45° layer and vice versa. The failed matrix material at this ±45° layer interface permits the fiber kinking to occur without significant fiber breakage.

When the matrix-shearing bands extend to the specimen edges, triangular wedges formed by the boundaries of these bands translate laterally. The change in specimen width for a failed $[(\pm 45)_{12}]_s$ laminate with a 2.54 cm diameter hole is shown in Fig. 12. The curve illustrates that specimen failure results in a significant change in specimen width in the region where a matrix-shearing band intersects the simply supported edge. This region is shaded on the curve and is labeled with y_1 or y_2. Similar deformation responses were

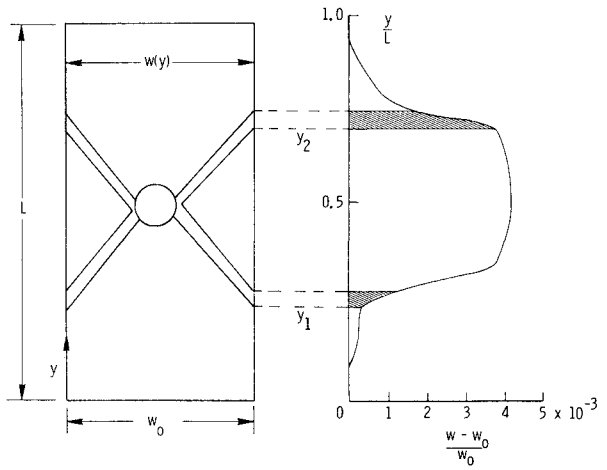

Fig. 12 Change in specimen width for a failed $[(\pm 45)_{12}]_s$ laminate with a 2.54 cm diameter hole.

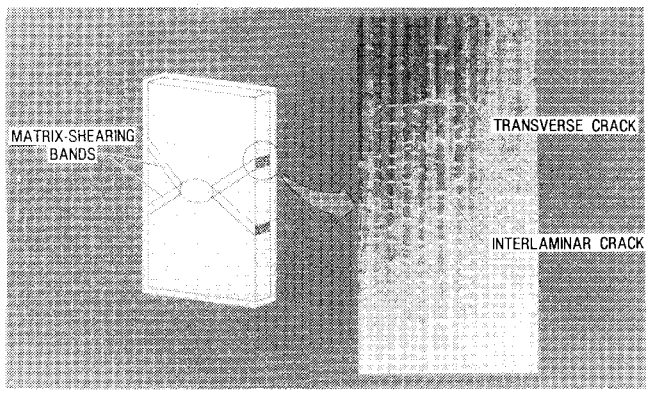

Fig. 13 Cracks at edge of failed $[(\pm 45/\mp 45)_6]_s$ laminate with a hole.

observed for laminates with other hole diameters and also for the glass-epoxy birefringent specimens.

A portion of the edge of a failed $[(\pm 45/\mp 45)_6]_s$ graphite-epoxy laminate with a hole is shown in Fig. 13. Interlaminar and transverse (through-the-thickness) cracks are observed throughout the laminate thickness at the simply supported edge but only within the region of the matrix-shearing bands (see the y_1 or y_2 region in Fig. 12). A gold-chloride solution was used to enhance observation of the cracks. The solution was applied to the hole boundary and infiltrated along $\pm 45°$ paths to the simply supported edge. Many laminates have a characteristic damage state that can be observed at the laminate edge.[13] The transverse cracks shown in Fig. 13 appear regularly spaced illustrating the characteristic damage state for this laminate and load condition.

The failure mechanism for the $\pm 45°$-dominated laminates with a hole differs from the failure mechanism for the all $\pm 45°$ laminates with a hole and was observed to be a combination of delamination and matrix shearing. As discussed for the $\pm 45°$-dominated control specimens, the 90° plies restrain in-plane shearing in the $\pm 45°$ plies. Also, the analytical results for the circular hole specimens showed that the shear stress concentration at the edge of the hole decreases as the percentage of 90° plies in the laminate thickness increases (Fig. 6c). For the laminates in this study, as the percentage of 90° plies in the laminate thickness is increased, the matrix-shearing contribution to failure appears to be reduced and an increase in the amount of delamination is observed.

Impact-Damaged Specimens

Experimental results for the laminates with impact damage are shown in Table 4. Data were obtained from specimens

Table 4 Compression failure data for laminates with impact damage

Laminate[a] (90° plies, %)	Laminate thickness, cm	Impact energy,[b] J	Major axis length of damaged region, cm	Failure stress, MPa	Failure strain, %
A (0)	0.66	5.7	2.36	180	1.36
	0.65	17.2	3.63	152	0.85
	0.65	36.0	5.99	118	0.60
C (8)	0.66	5.7	2.36	314	1.44
	0.67	17.0	3.63	174	0.73
	0.67	34.3	7.09	127	0.51
D (17)	0.68	5.5	2.54	275	1.41
	0.68	17.0	3.28	184	0.85
	0.68	35.1	6.17	131	0.56
E (25)	0.64	5.7	2.72	272	1.18
	0.65	16.6	4.17	145	0.59
	0.65	35.5	9.63	93	0.37
F (33)	0.67	5.5	2.18	274	1.17
	0.68	17.6	4.34	165	0.68
	0.67	34.3	7.98	113	0.44

[a]See Table 2 for stacking sequence. [b]No axial load was applied to specimen when impacted with 1.27 cm diameter aluminum sphere.

that were impacted at energy levels of approximately 5.5, 17.0, and 34.3 J and then loaded to failure. No visible damage was observed for specimens that were impacted at an energy level of 5.5 J; however, front- and back-side damage were observed at the impact location for specimens that were impacted at the higher energies.

Specimens with impact damage were C-scanned after impact but before compression loading, and typical results are shown in Fig. 14. Damage is indicated by the black regions on these photographs of the C-scans. The photographs show that specimens impacted at an energy level of 5.5 J had circular damaged regions with diameters of 2.2-2.7 cm (Fig. 14a). The C-scan results indicated that specimens impacted at other speeds had damaged regions that also were circular for laminate A (Fig. 14b), but were elliptical for the laminates with 90° plies (e.g., Fig. 14c). The major axis of the ellipse coincided with the fiber direction in the 90° plies. The ratio of the major axis length to the minor axis length for each ellipse increased as the percentage of 90° plies through the laminate thickness increased. The major axis length (diameter for circular regions) of the damaged regions was 3.3-4.3 and 6.0-8.0 cm for the specimens impacted at energy levels of 17.0 and 34.3 J, respectively. The length of the major axis measured on each specimen is reported in Table 4.

Compressive stress-strain data for impact-damaged laminates A and C-F are shown in Fig. 15. The results for laminates impacted at an energy level of 17.0 J are bounded by the results for the corresponding laminates impacted at energy levels of 5.5 and 34.3 J. The stress-strain response to failure for the laminates impacted at an energy level of 5.5 J is essentially the same as the stress-strain response for the corresponding control specimens (Fig. 2). Also, the failure stresses and strains for laminates A and C-F seem to be unaffected by impacting the laminates at an energy of 5.5 J. The laminate A impacted at an energy of 5.5 J and failed through the impact location; the failure was oriented at 45° to the load axis. The matrix-shearing mechanism noted previously for laminate A with a hole appears to be the primary failure mechanism for this impact-damaged laminate A. However, for laminates C-F impacted at an energy level of 5.5 J, failure was catastrophic and was initiated at sites outside the region with impact damage. By inspecting the failed specimens, the failure mechanisms for these impact-damaged laminates was observed to be a combination of matrix shearing and delamination.

The initial stress-strain response for the laminates impacted at energy levels of 17.0 and 34.3 J is essentially the

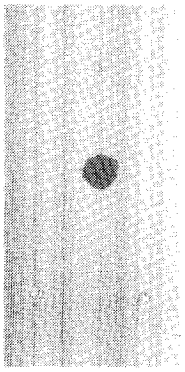

a) Laminate A, 0% 90° plies, 5.5 J impact energy.

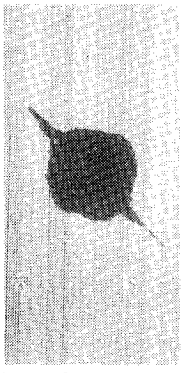

b) Laminate A, 0% 90° plies, 34.3 J impact energy.

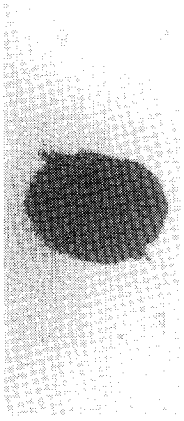

c) Laminate F, 33% 90° plies, 34.3 J impact energy.

Fig. 14 C-scan results for 25.4 cm long by 12.7 cm wide specimens after impact (all specimens impacted with a 1.27 cm diameter aluminum sphere).

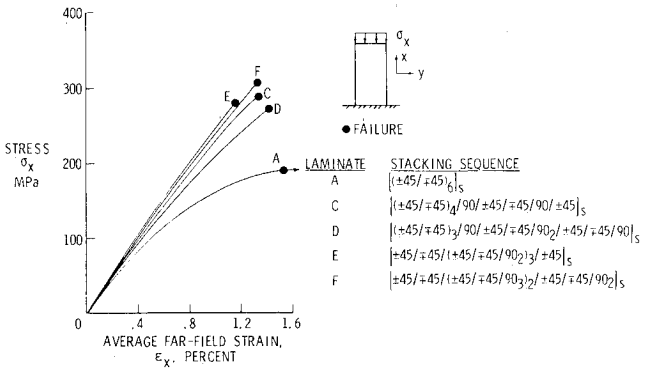

Fig. 15 Compressive stress-strain behavior for impact-damaged specimens.

same as the initial stress-strain response for the corresponding control specimens. However, the failure stress and corresponding strains for these impact-damaged specimens are significantly lower than those of the control specimens and are not a function of the percentage of 90° plies in the laminate. The failure stresses and strains for the laminates impacted at an energy level of 34.3 J were the lowest of the three energy levels tested. For the specimens impacted at energy levels of 17.0 or 34.3 J, failure was observed to initiate at the impact location and was catastrophic. The failure mechanism for these laminates is dominated by delamination, although matrix shearing was also observed.

Conclusions

An investigation was conducted to study the compression failure characteristics of ±45°-dominated graphite-epoxy laminates with a circular hole or impact damage. Control specimens (specimens without holes or impact damage), specimens with circular holes and specimens that had been subjected to impact damage were tested. All ±45° laminates and ±45°-dominated laminates with various percentages of 90° plies through the thickness were evaluated. The percentage of 90° plies was 8-33% of the laminate thickness. Also, two all ±45° glass-epoxy birefringent specimens, each with a single circular hole, were tested to study the laminate stress distribution and failure mode.

The failure mechanism for the ±45°-dominated laminates with a hole was different from the failure mechanism for the all ±45° laminate with a hole. In-plane shearing between the fiber and matrix (i.e., matrix shearing) was found to be the primary compression failure mechanism for an all ±45° laminate with a hole. C-scan photographs for graphite-epoxy laminates with a hole showed matrix-shearing bands that originated at the hole boundary and extended parallel to the fiber direction toward the specimen edges. Interlaminar and transverse (through-the-thickness) cracks were observed in the region where the matrix-shearing bands intersected the specimen edge. The failure mechanisms for the ±45°-dominated laminates with a hole was observed to be a combination of delamination and matrix shearing. Analytical results showed that for the shear stress oriented along the fiber direction, the shear stress concentration decreased as the percentage of 90° plies in the laminate increased. For the laminates tested in this study, the matrix-shearing contribution to failure appeared to be reduced and delamination was observed as the percentage of 90° plies in the laminate thickness was increased.

The compressive behavior of impact-damaged ±45°-dominated graphite-epoxy laminates was compared to the compressive behavior of impact-damaged all ±45° graphite-epoxy laminates. The compression failure stresses and strains and the failure mechanisms for both the all ±45° laminates and the ±45°-dominated laminates were unaffected by impacting the laminates at an energy level of 5.5 J with a 1.27 cm diameter aluminum projectile. The failure for the ±45°-dominated laminates was initiated at sites outside the region with impact damage. The failure stresses and strains for all the specimens impacted at an energy level of 17.0 or of 34.3 J were significantly lower than the corresponding data for the control specimens. The failure stresses and strains for these impact-damaged specimens were not a function of the percentage of 90° plies in the laminate. The failure mechanisms for these impact-damaged laminates was dominated by delamination, although matrix shearing also was observed.

References

[1] Starnes, J. H. Jr., Rhodes, M. D., and Williams, J. G., "Effect of Impact Damage and Holes on the Compressive Strength of a Graphite/Epoxy Laminate," *Nondestructive Evaluation and Flaw Criticality for Composite Materials,* edited by R. B. Pipes, ASTM STP 696, 1979, pp. 145-171.

[2]Rhodes, M. D and Williams, J. G., "Concepts for Improving the Damage Tolerance of Composite Compression Panels," NASA TM-85748, Jan. 1984.

[3]Garbo, S. P. and Ogonowski, J. M., "Strength Predictions of Composite Laminates with Unloaded Fastener Holes," *AIAA Journal*, Vol. 18, May 1980, pp. 585-589.

[4]Daniel, I. M., Niiro, T., and Koller, G. M., "Development of Orthotropic Birefringent Materials for Photoelastic Stress Analysis," NASA CR-165709, May 1981.

[5]Hong, C. S. and Crews, J. H. Jr., "Stress-Concentration Factors for Finite Orthotropic Laminates with a Circular Hole and Uniaxial Loading," NASA TP-1469, May 1979.

[6]Zimmerman, R. S., Adams, D. F., and Walrath, D. E., "Investigation of the Relations Between Neat Resin and Advanced Composite Mechanical Properties, Vol. I: Results," University of Wyoming, Laramie, Rept. UWME-DR-301-101-1, May 1983.

[7]Rhodes, M. D., Mikulas, M. M. Jr., and McGowan, P. E., "Effect of Orthotropic Properties and Panel Width on the Compression Strength of Graphite-Epoxy Laminates with Holes," AIAA Paper 82-0749, 1982.

[8]Freeman, S. M., "Characterization of Lamina and Interlaminar Damage in Graphite/Epoxy by the Deply Technique," *Composite Materials: Testing and Design (Sixth Conference)*, edited by I. M. Daniel, ASTM STP 787, 1982, pp. 50-62.

[9]Daniel, I. M., Rowlands, R. E., and Whiteside, J. B., "Effects of Material Stacking Sequence on Behavior of Composite Plates with Holes," *Experimental Mechanics*, Vol. 14, Jan. 1974, pp. 1-9.

[10]Rotem, A. and Hashin, Z., "Failure Modes of Angle Ply Laminates," *Journal of Composite Materials*, Vol. 9, April 1975, pp. 191-206.

[11]Yeow, Y. T., Morris, D. H., and Brinson, H. F., "The Fracture Behavior of Graphite/Epoxy Laminates," *Experimental Mechanics*, Vol. 19, Jan. 1979, pp. 1-8.

[12]Poe, C. C. Jr. and Sova, J. A., "Fracture Toughness of Boron/Aluminum Laminates with Various Proportions of 0° and ±45° Plies," NASA TP-1707, Nov. 1980.

[13]Reifsnider, K. L., "Some Fundamental Aspects of the Fatigue and Fracture Response of Composite Materials," *Recent Advances in Engineering Science*, edited by G. C. Sih, Lehigh University, Bethlehem, PA, 1977, pp. 373-384.